Applied Catalysis A: General 460–461 (2013) 15–20

Contents lists available at SciVerse ScienceDirect

Applied Catalysis A: General

journal homepage: www.elsevier.com/locate/apcata

Copper and nickel catalysts supported on praseodymium-doped ceria (PDC) for the water-gas shift reaction

Eduardo Poggio-Fraccari, Fernando Mariño, Miguel Laborde, Graciela Baronetti*

Laboratorio de Procesos Catalíticos, DIQ-FI, Universidad de Buenos Aires, Pabellón de Industrias, Ciudad Universitaria, 1428, Buenos Aires, Argentina

ARTICLE INFO

Article history:
Received 29 January 2013
Received in revised form 27 March 2013
Accepted 6 April 2013
Available online 19 April 2013

Keywords:
CO removal
Hydrogen
Ceria support
Praseodymium
Cu-Ni catalysts

ABSTRACT

The aim of this work is to study the behavior of Cu and Ni catalysts supported on praseodymium-doped ceria (PDC) for the WGS reaction. Samples were prepared by impregnation of several PDC supports (praseodymium content in the range 0–50 wt%) synthesized by the urea thermal decomposition method. Bare support and catalysts were characterized by BET, XRD, oxygen storage capacity and TPR. The activity tests were carried out in an atmospheric fixed bed reactor, using a $CO/H_2O/H_2/N_2$ mixture as the feed stream. Doping of ceria with small loading of Pr increases the surface reducibility and the oxygen storage capacity of ceria. Nickel catalysts are more active than copper ones. In both cases, catalysts supported on PDC with 5 Pr wt% are more active than samples supported on pure ceria. Methanation, which is likely to occur on Ni catalysts, is moderated in samples supported on praseodymium-doped ceria.

1. Introduction

Although water-gas shift (WGS) reaction has been extensively used in large chemical and petrochemical plants for more than 40 years, in the last years non-traditional applications of hydrogen (such as electric power generation in fuel cells) have given rise to new research efforts pointed to find active and stable catalysts for the WGS reaction.

Fuel cells for mobile sources (PEMFC) require that the inlet gas has a CO concentration lower than 20 ppm. Otherwise, the Pt-based anode is poisoned and the cell efficiency abruptly drops. Typically, a CO concentration of 6–8% is obtained at the outlet of the reformer unit when hydrogen is produced from a carbon containing raw material. Hence, a purification process must be carried out in order to reduce CO levels to cell requirements. So far, the most technologically feasible purification train consists of a water-gas shift converter, reducing CO from 8% to 1%, and a latter step of remaining CO elimination, until 20 ppm is reached. According to Zalc and Löffler [1], the WGS reactor is expected to have the largest volume since the intrinsic activity of WGS catalysts is low.

Traditionally, WGS reaction has been performed in two steps: the first, at high temperatures (HTWGS) using catalysts based in Fe and Cr; the second, at low temperatures (LTWGS), employing Cu-Zn-Al catalysts. This renewed interest in the study of WGS reaction has resulted in several works focused on finding alternative catalysts. Among these works, several authors taking into account the redox properties and the oxygen storage capacity of ceria, propose ceria-supported noble metal catalysts [2–4] or less expensive ceria-supported base metal catalysts [5–8]. More recently, it has been reported that redox and catalytic properties could be enhanced by doping the support with rare earths, especially La or Pr [9–11]. The aim of this work is to study the behavior of copper and nickel catalysts supported on praseodymium-doped ceria (PDC) for the WGS reaction. Transition metals were chosen based on some previous results indicating that Cu and Ni supported on pure ceria were active catalysts for CO oxidation by O_2 [12,13].

2. Experimental

CeO_2 and Pr-doped CeO_2 (PDC) tested in this work were obtained by thermal treatment of a precursor synthesized by the urea thermal decomposition method [14]. Precursors were prepared by aging cerium–praseodymium solutions ($Ce(NO_3)_3{\cdot}6H_2O$ and $Pr(NO_3)_3{\cdot}6H_2O$), mixed with urea, at 90 °C. During precipitation aliquots of solution were extracted and analyzed by MS-ICP in order to check the content of Ce and Pr.

Samples have been named CePr*X*, where *X* is the nominal molar percentage ratio of [Pr] to total cations ([Ce] + [Pr]) and varies between 0 (pure ceria) and 50. The calcination of these precursors was carried out in air at 450 °C for 5 h.

Catalysts were prepared by incipient impregnation of ceria-based supports, obtained as previously described, with the corresponding metal salts: $Cu(NO_3)_2{\cdot}_3H_2O$ or $Ni(NO_3)_2{\cdot}6H_2O$. After

* Corresponding author. Tel.: +54 011 4576 3240.
E-mail addresses: baroneti@di.fcen.uba.ar, gra.baronetti@gmail.com (G. Baronetti).

0926-860X/$ – see front matter © 2013 Elsevier B.V. All rights reserved.
http://dx.doi.org/10.1016/j.apcata.2013.04.013

the impregnation procedure, catalysts were dried in a stove at 70 °C for 24 h and subsequently calcined following the same thermal treatment procedure as the CePr*X* supports. All the catalysts presented in this work were prepared with metal contents of ca. 18 wt% of Cu, Ni or the same total content of metal in case of bimetallic catalyst. These bimetallic samples were synthesized with a constant total metal loading of 18 wt.% with two copper to nickel molar ratios, (Cu:Ni 1:1 named Cu-Ni(1–1)/CePr15 and Cu:Ni 1:3 named Cu-Ni(1–3)/CePr15). All solids were dissolved in acidic solutions in order to extract the metal and further analyze these solutions by MS-ICP. BET values were obtained with a Micromeritics ASAP2020 instrument.

The samples were characterized by powder X-ray diffraction (XRD) using the graphite-filtered Cu Kα radiation (λ = 1.5406 Å).

Temperature-programmed reduction experiments were performed in a Micromeritics Auto Chem II 2920 instrument equipped with TCD detector an coupled to a Pfeiffer vacuum mass spectrometer; an H_2/Ar stream (4% H_2, 50 cm^3/min) was passed over 30 mg of the catalytic samples (120 mg in the case of bare supports) while operation temperature was raised from RT to 400 °C (1000 °C for supports) using a rate of 10 °C/min. Prior to TPR tests the samples were treated at 450 °C for 1 h under air flow to clean the surface.

Oxygen storage capacity (OSC) measurements were performed by injecting alternating pulses of CO and Air at 400 °C using the Micromeritics Auto Chem II 2920 apparatus described before, and following the CO, CO_2 and O_2 signals by mass spectrometry [15].

Activity tests were conducted in a fixed bed glass reactor using 120 mg of catalyst and a total inlet flow of 150 cm^3/min; in the case of bare supports, tests were performed with 240 mg and a flow of 85 cm^3/min. Feed stream contains CO (8%), H_2O (24%), H_2 (45%) and N_2 as balance. The catalytic performance was evaluated at several temperatures in the range 250–450 °C. Before each analysis, solids were reduced during 0.5 h with an H_2 stream (50% of H_2 in N_2) at the higher temperature of reaction. At the reactor outlet, analysis of non-converted CO and gaseous products was performed by a Hewlett Packard HP 6890 gas chromatograph equipped with a TCD detector. Reported values of CO conversion correspond to steady state values.

3. Results and discussion

3.1. Characterization and WGS activity of ceria and praseodymium-doped ceria (PDC) supports

3.1.1. Precipitation and composition of supports

During precipitation, the fractions of Ce and Pr in solution were followed by extracting small quantities of solutions and analyzing the content of both elements. As an example, Fig. 1 shows the results for CePr15 sample. It can be observed that after 9 h all cations have precipitated. The composition of the solids obtained after 24 h of precipitation were studied. All samples were dissolved into acidic solutions and analyzed by MS-ICP. The composition of the solids is close to the nominal value for low Pr content but is lower for higher Pr content, Table 1.

3.1.2. Surface area

Table 1 displays BET results of CePr*X* supports. As it can be seen, surface areas of samples with praseodymium content up to 15 wt% are similar to that of pure ceria. On the contrary, a marked diminution of surface area can be noticed in sample CePr50. Using BET results, Table 1 presents an estimation of the particle size assuming spherical shape according to the following equation [16]

$$D_{BET} = \frac{6}{\rho S_{BET}} \quad (1)$$

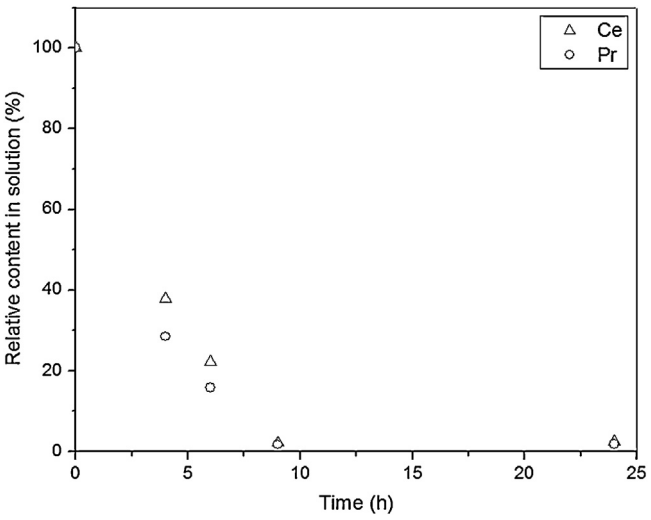

Fig. 1. Ce and Pr fraction in solution during precipitation of CePr15 sample.

where D_{BET} is the particle size, S_{BET} is the BET surface area of samples and $\rho = 7.2\ g/cm^3$ represents the theoretical density of CeO_2 (for PDC we use the same value since the atomic weights of Pr and Ce are very similar and, therefore, lattice contraction or expansion is expected to be negligible).

3.1.3. X-ray diffraction

XRD patterns of pure and doped ceria samples (Fig. 2) present the characteristic reflections of solids with fluorite-type structure, corresponding to the planes (1 1 1), (2 0 0), (2 2 0), (3 1 1), (2 2 2), (4 0 0), (3 3 1), (4 2 0), (4 2 2) and (5 1 1) [17].

There is no evidence of pure praseodymium phase segregation by this technique. A detailed analysis of the position of the XRD peaks would provide additional information about the structure of the ceria-based supports, as the position of the peak (1 1 1) shifts to higher or lower angles due to contraction or expansion of the unit cell [18,19]. Nevertheless, in the case of our CePr*X* samples, the position of the peak (1 1 1) does not significantly change because the Ce^{4+} ionic radius (0.097 nm) is very similar to that of Pr^{4+} (0.096 nm) [10,20]. The crystallite sizes, which were estimated by Scherrer's equation and presented in Table 1, are similar for all samples. However, the average number of crystallites by particle,

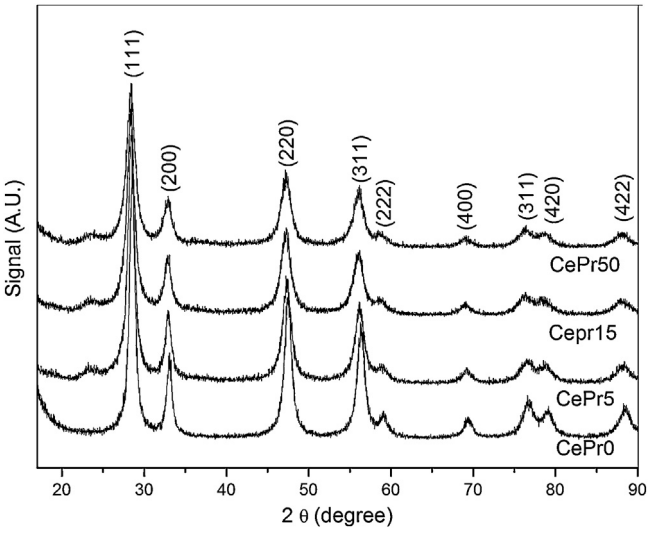

Fig. 2. X-ray diffraction patterns of PDC supports.

Table 1
Chemical analysis, BET and XRD results of PDC supports.

Sample	Content of Pr (%)[a]	S_{BET} (m^2/g)	D_{BET} (nm)[b]	D_{XRD} (nm)	$(D_{BET}/D_{XRD})^3$
CePr0	–	110.1	7.6	8.1	0.8
CePr5	4.7	100.2	8.3	8.4	1
CePr15	13.0	89.4	9.3	7.4	2
CePr50	39.0	19.4	43.0	6.4	303

[a] Calculated by results of MS-ICP.
[b] Calculated by Eq. (1).

estimated by the ratio $(D_{BET}/D_{XRD})^3$, is much higher for CePr50 than for the other supports, as it can be seen in the last column of Table 1. This result indicates that the decrease in BET values is related to an agglomeration of the crystallites.

3.1.4. Temperature programmed reduction

Fig. 3 shows the H_2-TPR profiles of the CeO_2-based supports. Pure CeO_2 exhibits two reduction events ("bimodal curve"). The first signal located at ca. 470 °C (α peak) was assigned to the reduction of the most reducible surface oxygen atoms, while the high temperature signal (β peak at ca. 830 °C) corresponds to the reduction of the bulk oxygen atoms [17].

For CePr*X* samples, the temperature of maximum H_2 consumption in α peaks is very similar to that of pure ceria except for sample CePr50 where the position of α peak shifts approximately 70 °C to lower temperatures. In addition, as Pr content increases, profiles of CePr*X* samples show differences in both the α and β regions with respect to pure ceria. First, the H_2 consumption at higher temperatures (β peak ca. 800 °C) notably decreases in agreement with other authors [20,21]. For all the samples (including CePr0), one or more reduction events take place at temperatures lower than that of α peak. Nevertheless, these features below 350 °C become notably visible for samples CePr15 and CePr50 with respect to CePr0. Thus, it can be concluded that CePr*X* samples are more reducible than the pure CeO_2 in this temperature range [20]. Furthermore, the net amount of hydrogen consumed in these low temperature peaks increases as praseodymium content also increases. This behavior has associated with the reduction of Pr^{4+} to Pr^{3+} at the surface region [22,23].

3.1.5. WGS activity and OSC measurements

The catalytic activity of the PDC supports is shown in Fig. 4 in terms of the rate of WGS reaction per catalyst mass unit at 450 °C. The activity of the samples increases when a small amount of praseodymium is added to ceria support. It has been proposed that WGS reaction proceeds via a co-operative redox mechanism over catalysts supported on oxides which are active for oxygen transport and storage [24]. In this sense, Fig. 4 also shows that the activity data are in good agreement with the oxygen storage capacity of the samples. Therefore, the enhanced activity is explained by the better oxygen mobility in the oxides. Similar results were obtained for ternary oxides Ce–Pr–Zr by Cao et al. [25], in which a correlation between OSC and H_2/CO ratio (by WGS reaction) was observed. It must be noted that the support with the highest Pr content (CePr50) shows the lowest activity and OSC, and this sample has a very low surface area. Rossignol et al. [19] have explained the correlation between OSC and BET values through a theoretical calculation of the OSC considering only geometric parameters, i.e. a ratio between surface area and a square lattice parameter for the samples.

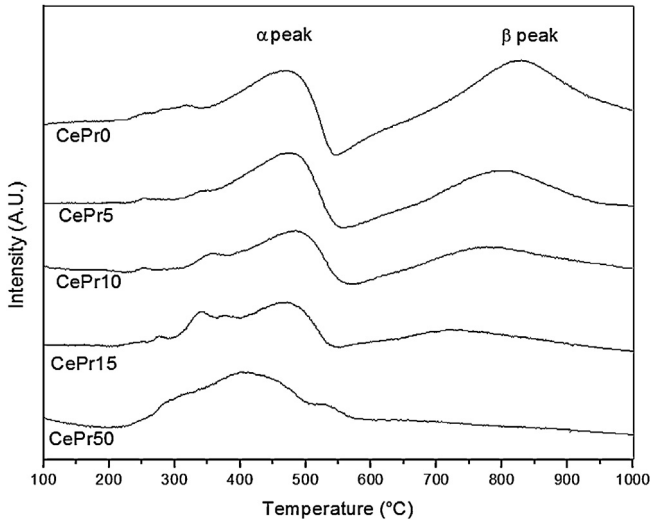

Fig. 3. TPR profiles of PDC supports.

3.2. Reducibility and catalytic activity of Cu and Ni catalysts supported on PDC

3.2.1. Temperature programmed reduction

Fig. 5a and b shows the TPR profiles of Cu and Ni catalysts, respectively. Comparing these profiles with those of Fig. 3, it can be seen that Cu catalysts show completely different reduction profiles with respect to that of the bare supports. In fact, low temperature (150–250 °C) peaks are not observed on PDC supports as it can be seen in copper catalysts (Fig. 5a).

In similar experimental conditions, pure CuO profile exhibits a single reduction peak centered at ca. 320 °C [26]; this temperature is markedly higher than the temperatures of the reduction events of any of the copper catalysts. Therefore, the reducibility of copper is significantly promoted in Cu catalysts supported in PDC. From the comparison between different profiles, it can be noted an increase of the temperature at which reduction events take place for samples with Pr content higher than 5%. In general, catalysts show more than one reduction event, suggesting the presence of different copper species and/or partial reduction of the support; particularly, samples supported on CePr0 and CePr5 present reduction peaks at very low temperatures (even lower than 150 °C). As it is reported in the next section, these samples are also the most active catalysts for WGS reaction. Concerning Ni catalysts, reduction temperatures observed in Fig. 5b for PDC-supported catalysts

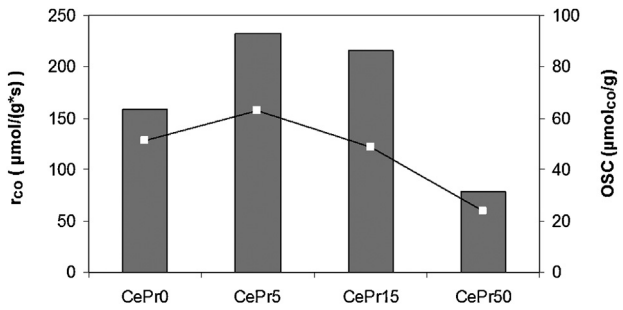

Fig. 4. WGS activity and oxygen storage capacity of PDC supports.

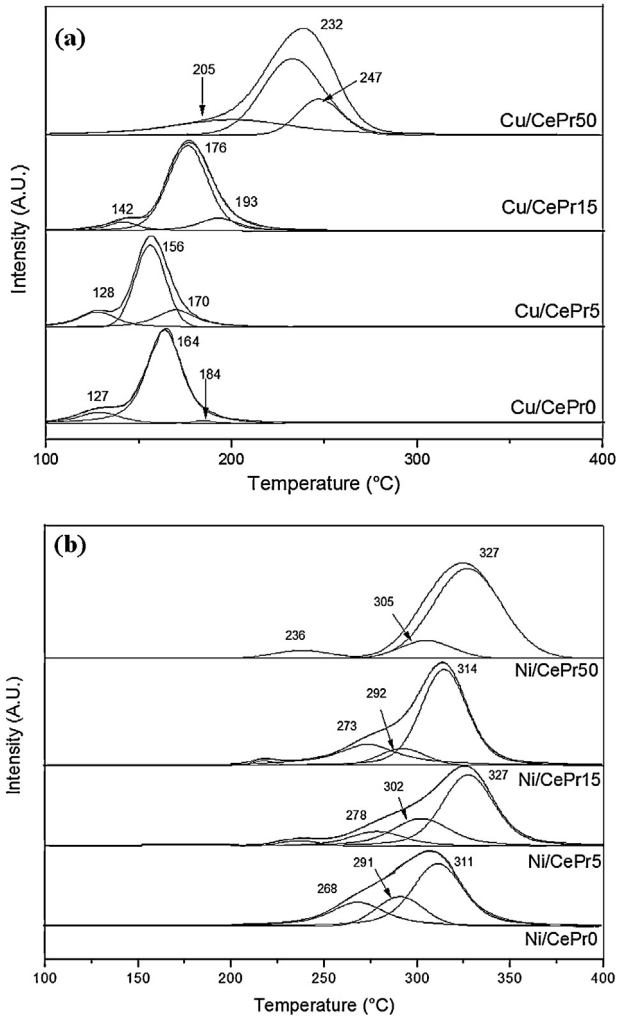

Fig. 5. TPR profiles of catalysts supported on PDC: (a) copper catalysts; (b) nickel catalysts.

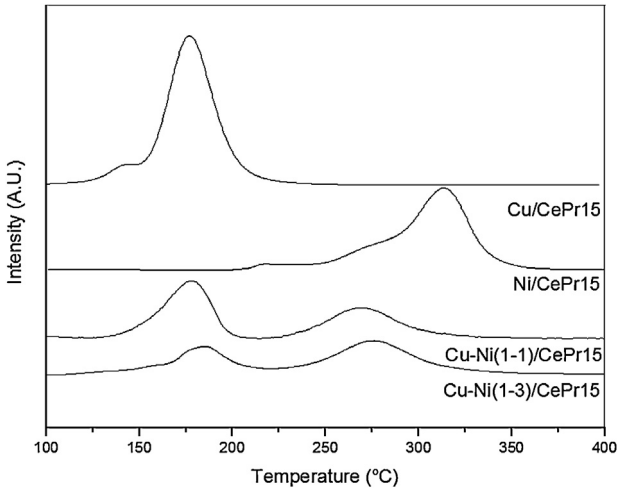

Fig. 6. TPR profiles of copper-nickel and monometallic catalysts supported on CePr15.

are lower than the reduction temperature found for pure NiO in similar conditions (400 °C), as reported by Chary et al. [27].

Table 2 shows the total amount of water produced in the reduction processes at low temperatures (range of temperatures showed in Fig. 5) and the theoretical amount of H_2O that would be produced due to the complete reduction of CuO to Cu^0 or NiO to Ni^0 in each sample, as calculated from the Cu or Ni contents determined by ICP. As it can be seen, H_2O production estimated from TPR consumption peaks is higher than the corresponding stoichiometric values in the case of copper catalysts, suggesting some reduction

Table 2
H_2O production from TPR experiments with stoichiometric amount of H_2O produced from the reduction processes $Cu^{2+} \rightarrow Cu^0$ or $Ni^{2+} \rightarrow Ni^0$ and OSC results as consumption of CO per gram of catalysts.

Sample	TPR H_2O production (μmol)	Theoretical H_2O production (μmol)	OSC (μmol CO/g)
Cu/CePr0	90.2	67.9	256
Cu/CePr5	84.1	67.9	208
Cu/CePr15	98.8	67.9	292
Cu/CePr50	159.2	67.9	298
Ni/CePr0	67.6	72.3	136
Ni/CePr5	67.6	72.3	110
Ni/CePr15	76.1	72.3	179
Ni/CePr50	109.6	72.3	70
Cu-Ni(1–3)/CePr15	62.6	69.5	236
Cu-Ni(1–1)/CePr15	59.4	70.6	213

of the Ce and/or Pr ions. This behavior is not observed for nickel catalysts except for the sample with higher Pr content, Ni/CePr50. As it can be seen in Fig. 3, the reduction of CePr50 starts at a lower temperature compared to the other supports (ca. 250 °C). Fig. 5b shows that the most important reduction event of Ni/CePr50 catalyst also occurs close to this temperature. Therefore, data reported in Table 2 suggest that Ce and Pr reduction probably takes place to some extent in the case of Ni/CePr50 sample. A peak fitting of the profiles was performed in order to identify the temperature of the different reduction events. In the case of Cu catalysts, three peaks were found for each sample. Several authors attribute the events at low temperature to the reduction of dispersed copper entities strongly interacting with ceria; the high temperature events were assigned to the reduction of copper species with poor interaction with the support [28–30] and to a partial (superficial) reduction of the support (Table 2). Nickel catalysts have shown a very broad profile related to the reduction of different nickel species. According to some authors [27,31], high temperature events were assigned to species with stronger interaction with the support; however, reduction peaks at high temperatures have also been ascribed to the reduction of free NiO particles or clusters on the support [24,32].

In the case of bimetallic catalysts two well separated peaks were found in the profiles shown in Fig. 6, one at low temperature (150–200 °C) and the other at higher temperatures (250–300 °C). As it can be seen, the first peak in bimetallic catalysts takes place in the same temperature range than the main event in Cu/PDC catalysts; nevertheless, the second peak in bimetallic samples has its maximum at lower temperatures compared to Ni/PDC catalysts. These might imply that although the reducibility of copper is not affected in bimetallic samples, metallic copper catalyzes the reduction of NiO. This effect has also been observed by Lin at al [33] for their copper-nickel catalysts supported over ceria-lanthana.

3.2.2. Oxygen storage capacity measurements

The OSC results reported are the average of five reduction/oxidation cycles. All the values shown in Table 2 were higher than those obtained for the supports (Fig. 4) indicating a promoting effect of both metals over the OSC of bare supports [34]. In agreement with other authors [35], copper containing samples have more labile oxygen (higher OSC) than nickel catalysts, and bimetallic samples show intermediate values. In Section 3.1.5 the highest oxygen storage capacity was found for a support with a low Pr content (CePr5), while the results for copper containing catalysts do not show the same trend. The higher OSC value found for Cu/CePr50

Table 3
Crystallite sizes of copper particles in fresh and used catalysts.

Sample	Crystallite size (nm)	
	CuO	Cu^0
Cu/CePr5	26.0	–
Cu/CePr5 (used)	–	29.2
Cu/CePr50	19.1	–
Cu/CePr50 (used)	–	35.1

with respect to Cu/CePr5 could be explained by a better copper dispersion in the former, as it is shown by the CuO crystallite size reported in Table 3, which were estimated using XRD patterns of Fig. 7.

3.2.3. WGS activity

Fig. 8a and bshows the WGS light-off curves for the copper and nickel based catalysts tested in this work. As it can be seen, Ni-containing catalysts (Fig. 8b) are more active than the samples containing copper (Fig. 8a), especially at high temperatures. Moreover, it can be seen that the slope in the light–off curves of the Ni-containing catalysts are more sharply than the slope of the copper catalysts. As a consequence, copper catalysts seem to be similar to Ni-containing catalysts at low CO conversions and low temperatures, but, when the reaction temperature is increased, higher CO conversions are obtained with Ni-containing catalysts.

In both cases, for copper and nickel catalysts, the better catalytic performances are found on samples supported on PDC with low Pr content.

The best copper catalyst was the sample supported on CePr5, in coincidence with the highest activity of CePr5 mixed oxide among the supports. In addition, WGS activity correlates well with the OSC for the bare supports in Fig. 4, but this is not the case for Cu catalysts; for example, Cu/CePr50 sample presents the highest OSC value in Table 2, but its WGS activity is markedly lower than that of Cu/CePr5 catalyst.

XRD patterns of fresh and used Cu/CePr5 and Cu/CePr50 catalysts are presented in Fig. 8, together with XRD patterns of the supports. Peaks corresponding to CuO are found in both fresh samples and metallic copper signals are observed in both samples after being tested in the WGS reaction. The presence of Cu^0 in the exhausted samples is expected due to the reduction treatment performed before each catalytic run. However, it can be seen in Table 3 that the growth of copper crystallites clearly depends on Pr

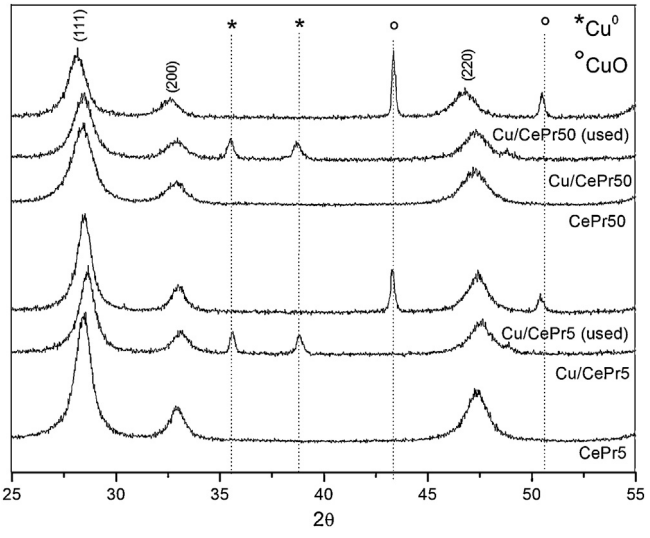

Fig. 7. XRD patterns of fresh and used Cu catalysts over CePr5 and CePr50.

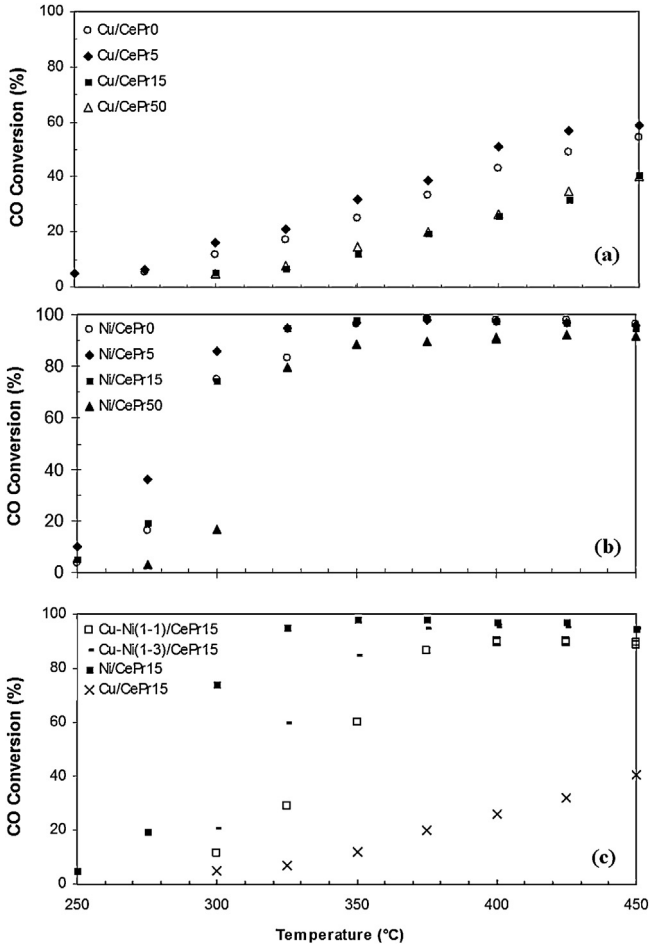

Fig. 8. CO conversion in WGS reaction as a function of the operation temperature for catalysts supported on PDC: (a) copper catalysts; (b) nickel catalysts; (c) copper-nickel catalysts.

content. In effect, the presence of water in the feed stream during WGS runs provokes textural changes, being this effect much more pronounced in the case of Cu/CePr50 sample. This last result could explain the low catalytic activity of Cu/CePr50 sample in spite of its high OSC value.

To confirm this observation, WGS runs with different water content in the feed were performed. CO conversions obtained with Cu/CePr5 and Cu/CePr50 samples are reported in Table 4. For both catalysts, CO conversion increases as water concentration in the feed also increases which verifies a positive reaction order with respect to water already reported by other authors for similar catalysts [6]. Nevertheless, this effect is much less marked in the case of Cu/CePr50 catalyst, indicating the negative effect of water on the structure of this sample.

Methanation reactions could take place on these catalysts, reducing the amount of hydrogen produced. For the copper catalysts analyzed, not even traces of methane were detected at the reactor outlet in any experience [12]. On the contrary, Table 5

Table 4
Results of water-gas shift runs with different feed water content.

Sample	CO conversion (%) at 450 °C with CO:H_2O		CO conversion (%) at 400 °C with CO:H_2O	
	1:1	1:3	1:1	1:3
Cu/CePr5	35	56	28	41
Cu/CePr50	24	40	19	26

Table 5
Selectivity of Ni catalysts at different temperatures.

Sample	Selectivity (mol_{CO2}/mol_{CH4})	
	450 °C	350 °C
Ni/CePr0	0.5	0.6
Ni/CePr5	0.9	0.8
Ni/CePr15	0.8	0.7
Ni/CePr50	1.1	0.9
Cu-Ni(1–3)/CePr15	0.5	1.7
Cu-Ni(1–1)/CePr15	2.5	3.0

shows that methanation reactions are important on nickel catalysts. Praseodymium doping enhances the selectivity towards WGS reaction since the Ni catalyst supported on pure ceria presents the more significant value of methane production.

Taking into account this fact, we prepared bimetallic catalysts of copper and nickel and tested them in the WGS reaction with the objective of obtaining both good activity and an acceptable selectivity. These catalysts were prepared over the CePr15 support since Ni/CePr15 sample has showed the highest activity but a poor selectivity.

Fig. 8c reports CO conversion for bimetallic catalysts and those obtained with monometallic copper or nickel catalysts for the sake of comparison. It can be seen that bimetallic samples exhibit better conversion than copper catalyst but lower conversion than nickel catalyst. Selectivity values reported in Table 5 indicate a higher selectivity for Cu-Ni(1–1)/CePr15 sample, while the selectivity of Cu-Ni(1–3)/CePr15 sample is similar to that of monometallic Ni catalyst. The replacement of Ni by Cu over the support keeps an acceptable WGS activity without promoting methanation. In particular, Table 5 indicates that sample Cu-Ni(1–1)/CePr15 allows reducing CO concentration from 8% in the feed to approximately 1% with selectivity close to 3, i.e. virtually without net H_2 lose during the reaction.

4. Conclusions

Copper and nickel catalysts supported on praseodymium-doped ceria (PDC) were prepared, characterized and evaluated for the WGS reaction in the 250–450 °C temperature range. Concerning bare supports, doping with small loadings of Pr (5 Pr wt.%) increases the reducibility and the oxygen storage capacity of ceria. Nickel catalysts show to be more active than copper catalysts, particularly at high temperatures. Under our operation conditions, Ni catalysts supported on CePr0, CePr5 and CePr15 supports are able to achieve equilibrium CO conversions for temperatures higher than 350 °C. Cu and Ni catalysts supported on PDC with 5 Pr wt% are more active than samples supported on pure ceria. Methanation is likely to take place over Ni-containing catalysts, but this tendency to CO and CO_2 methanation is partially reduced in catalysts supported on praseodymium-doped ceria and bimetallic catalysts. In fact, the catalyst with a Cu-Ni 1–1 molar ratio supported on PDC with 15 wt% Pr has shown a CO conversion of 85% (less than 1% mol/mol of CO in the exhaust of the reactor) and a CO_2/CH_4 selectivity close to 3/1 in a temperature range of 350–450 °C, according to the main objective of this work.

Acknowledgements

To the University of Buenos Aires (UBA), SECyT, ANPCyT and CONICET for their financial support.

References

[1] J.M. Zalc, D.G. Löffler, J. Power Sources 111 (2002) 58–64.
[2] G. Jacobs, E. Chenu, P. Patterson, L. Williams, D. Sparks, G. Thomas, B. Davis, Appl. Catal. A: Gen. 258 (2004) 203–214.
[3] A. El-Moemen, A. Karpenko, Y. Denkwitz, R. Behm, J. Power Sources 190 (2009) 64–75.
[4] L. Mattos, F. Noronha, J. Power Sources 145 (2005) 10–15.
[5] N. Koryabkina, A. Phatak, W. Ruettinger, R. Farrauto, F. Ribeiro, J. Catal. 217 (2003) 233–239.
[6] X. Qi, M. Flytzani-Stephanopoulos, Ind. Eng. Chem. Res. 43 (2004) 3055–3062.
[7] P.V.D.S. Gunawardana, H.C. Lee, D.H. Kim, Int. J. Hydrogen Energy 34 (2009) 1336–1341.
[8] D. Gamarra, A. Hornés, Z. Koppany, Z. Schay, G. Munuera, J. Soria, A. Martínez-Arias, J. Power Sources 169 (2007) 110–116.
[9] B. Reddy, L. Katta, G. Thrimurthulu, Chem. Mater. 22 (2010) 467–475.
[10] S. Parres-Esclapez, M.J. Illán-Gómez, C. Salinas-Martínez de Lecea, A. Bueno-López, Appl. Catal. B: Environ. 96 (2010) 370–378.
[11] M. Małecka, L. Kepinski, W. Mista, Appl. Catal. B: Environ. 74 (2007) 290–298.
[12] F. Mariño, C. Descorme, D. Duprez, Appl. Catal. B: Environ. 58 (2005) 175–183.
[13] N. Ribeiro, M. Souza, M. Schmal, J. Power Sources 179 (2008) 329–334.
[14] M. Jobbágy, F. Mariño, B. Schönbrod, G. Baronetti, M. Laborde, Chem. Mater. 18 (2006) 1945–1950.
[15] H. Yao, Y. Yao, J. Catal. 86 (1984) 254–265.
[16] F. Mariño, G. Baronetti, M. Laborde, N. Bion, A. Le Valant, F. Epron, D. Duprez, Int. J. Hydrogen Energy 33 (2008) 1345–1353.
[17] E. Poggio, M. Jobbágy, M. Moreno, M. Laborde, F. Mariño, G. Baronetti, Int. J. Hydrogen Energy 36 (2011) 15899–15905.
[18] F. Zhang, S. Chan, J. Spanier, E. Apak, Q. Jin, R. Robinson, I. Herman, Appl. Phys. Lett. 80 (2002) 127–129.
[19] S. Rossignol, C. Descorme, C. Kappenstein, D. Duprez, J. Mater. Chem. 11 (2001) 2587–2592.
[20] M. Luo, Z. Yan, L. Jin, J. Mol. Catal. A: Chem. 260 (2006) 157–162.
[21] P. Fang, M. Luo, J. Lu, S. Cen, X. Yan, X. Wang, Thermochim. Acta 478 (2008) 45–50.
[22] R. Long, J. Luo, M. Chen, H. Wan, Appl. Catal. A: Gen. 159 (1/2) (1997) 171–185.
[23] C. Lopez-Cartes, S. Bernal, J. Calvino, M. Cauqui, G. Blanco, J. Perez-Omil, J. Pintado, S. Helveg, P. Hansen, Chem. Commun. 5 (2003) 644–645.
[24] Y. Li, Q. Fu, M. Flytzani-Stephanopoulos, Appl. Catal. B: Environ. 27 (2000) 179–191.
[25] L. Cao, C. Ni, Z. Yuan, S. Wang, Catal. Commun. 10 (2009) 1192–1195.
[26] X. Tang, B. Zhang, Y. Li, Y. Xu, Q. Xin, W. Shen, Appl. Catal. A: Gen. 288 (2005) 116–125.
[27] K. Chary, P. Rao, V. Vishwanathan, Catal. Commun. 7 (2006) 974–978.
[28] W. Liu, M. Flytzani-Stephanopoulos, J. Chem. Eng. 64 (1996) 283–294.
[29] D. Ratnasay, D. Srinivas, C. Satyanarayana, P. Manikandan, R. Kumaran, M. Sachin, N. Shetti, J. Catal. 221 (2004) 455–465.
[30] X. Zheng, X. Zhang, X. Wang, S. Wang, S. Wu, Appl. Catal. A: Gen. 295 (2005) 142–149.
[31] Y. Zhang, J. Zhou, Y. Chen, Z. Wang, J. Liu, K. Cen, Int. J. Hydrogen Energy 33 (2008) 5477–5483.
[32] Y. Li, B. Zhang, B. Tang, Y. Xu, W. Shen, Catal. Commun. 7 (2006) 380–386.
[33] J. Lin, P. Biswas, V. Guliants, S. Misture, Appl. Catal. A: Gen. 387 (2010) 87–94.
[34] S. Bedrane, D. Descorme, D. Duprez, Catal. Today 73 (2002) 233–238.
[35] S. Kacimi, J. Barbier, R. Taha, D. Duprez, Catal. Lett. 22 (1993) 343–350.